Draft version July 25, 2017
Typeset using LaTeX **twocolumn** style in AASTeX61

CONNECTING THE REIONIZATION HISTORY OF GALAXIES TO THEIR Z=0 PROPERTIES

Dominique Aubert,[1] Pierre Ocvirk,[1] Nicolas Deparis,[1] INCITE,[1] and CLUES[1]

[1] *Observatoire Astronomique de Strasbourg*
11 rue de l'Universite
67000, Strasbourg, France

Submitted to ApJL

ABSTRACT

We present predictions of the Reionization times of z=0 galaxies, made using simulations. The $z > 6$ epoch is described using a radiative hydrodynamics simulation produced with the AMR code EMMA and deployed on 32768 CPU cores and 4096 GPUs on Titan. High-redshift predictions are projected 13 billions years later using a pure dark matter Gadget simulation with the same set of initial conditions. In both cases the $(64\mathrm{Mpc/h})^3$ volume is sampled with $2048^3 \sim 8 \times 10^9$ initial resolution elements, allowing to probe halos in the $10^8 - 10^{13} M_\odot$ range.

We find that current massive galaxies ($> 10^{12} M_\odot$) were reionized $\sim 200 \times 10^6$ years earlier than the Universe as a whole, resulting from these objects being the hosts of the first sources. The scatter in Reionization times can be quite significant and Milky-Way like galaxies can have z=6 progenitors reionized as early as z=13 and as late as z=8. Less massive objects ($< 10^{12} M_\odot$) are reionized at the same time as the overall volume or even later : this lag can be attributed to dark objects that require external radiation to complete their reionization. Measures of the reionization durations within halos show that the amount of time required to reionize galaxies can be as large as the halo-to-halo fluctuation of reionization times. Finally, we compare reionization times and durations in sub-volumes with different densities : overdense regions promote earlier and faster Reionizations.

Keywords: dark ages, reionization, first stars — galaxies: high-redshift — methods: numerical

Corresponding author: Dominique Aubert
dominique.aubert@astro.unistra.fr

1. INTRODUCTION

The emergence of a UV background during the Reionization sets the thermal and ionisation state of the intergalactic medium. It can also suppress star formation in the progenitors of galaxies through photo-heating especially for low-mass objects below $10^9 M_\odot$. Accordingly, reconstructed star formation histories of the faintest dwarf galaxies indicate that the Reionization stopped the build up of their stellar populations (see e.g. Brown et al. (2014)). Likewise recent radiative hydrodynamics simulations were able to reproduce this suppression in large high resolution simulations (Ocvirk et al. 2016).

However, the Reionization is not a uniform and instantaneous process: by the mere presence of AGNs (see e.g. Chardin et al. (2015)) or nearby clusters (see e.g. Iliev et al. (2011)), variations in the transition properties are expected, with important consequences on models predictions. In particular, assigning a single Reionization epoch for both the IGM and proto-galaxies is incorrect. The timing of the Reionization can have an impact on e.g. the satellite populations of z=0 galaxies (see e.g. Koposov et al. (2009); Busha et al. (2010); Ocvirk & Aubert (2011); Iliev et al. (2011); Ocvirk et al. (2014); Gillet et al. (2015)) and the assumption on extended or instantaneous reionization has a dramatic impact on the stellar populations of satellite galaxies. In a global context where the exact contribution of small galaxies to the Reionization is debated (see e.g. Bouwens et al. (2014); Finkelstein et al. (2015)), all these aspects push for an improved description of the transition as seen from the high-z galaxies.

It also raises the question of linking the physics of the EoR to galaxies seen in the contemporary Universe. 13 billions years separate the Reionization from today and given the variety of build-up histories, it's not an easy task to determine the reionization context of a $z \ll 6$ galaxy. In the current letter, we explore the timings of the Reionization of $z = 0$ galaxies using a EMMA radiative hydrodynamics simulation of the Reionization (Aubert et al. 2015) and extrapolating $z > 6$ properties to $z = 0$ using a pure DM Gadget simulation that shares the same initial conditions. We focus on the time and duration of the Reionization and we investigate briefly the impact of cosmic variance. The work presented here follow the lines of previous studies made by e.g. Alvarez et al. (2009) and Li et al. (2014) who focused on scales and masses relevant for large galaxies or clusters, using a semi-numerical methodology. Here we focus on smaller objects with masses between $10^8 M_\odot$ and $10^{13} M_\odot$ and our methodology is entirely based on simulations. Our methodology is also similar to Ocvirk et al. (2014) on the Local Group Reionization. However, in the current letter we focus on the population of galaxies in a large cosmological volume rather than a specific object. Furthermore our reionization predictions rely on a self-consistent radiative hydrodynamics calculations instead of radiative post-processing techniques. As shown hereafter, our results are consistent with both these previous large/cluster-scale and local group focused studies.

We first present our set of simulations and the analysis performed. As detailed in the Result section, we find that the reionizations of z=0 galaxies present a great variability as a function of their masses and within a given class of mass. We conclude by discussing the implications of the current results and future route for more detailed investigations.

2. METHODS

2.1. *Initial Conditions*

The initial conditions were created by the CLUES collaboration and assume a WMAP 5 cosmology ($\Omega_m = 0.279, \Omega_v = 0.721, H_0 = 70$ km/s/Mpc, Hinshaw et al. (2009)). They cover a 64 Mpc/h comoving volume with a 2048^3 sampling. The initial phases were chosen to produce an analog of the Local Universe at z=0 (see Gottloeber et al. (2010),Iliev et al. (2011)) but this feature won't be addressed here. These choices were motivated by future comparisons with the CODA I simulation (Ocvirk et al. 2016).

2.2. *Simulations*

The $z > 6$ predictions of this project were produced by the AMR simulation code EMMA (Aubert et al. 2015). It tracks the coupled collisionless dynamics, hydrodynamics and radiative transfer and includes standard subgrid models for star formation and supernovae feedback (Deparis et al. (2017), in prep.).

Space is sampled on a 2048^3 grid that gets refined if it contains more than 8 DM particles. The grid is prevented to refine to physical resolutions smaller than 500 pc, corresponding to 3 additional levels of refinement by z=6 : the actual number of cells is then multiplied by 2.1, i.e. 18 billions cells.

Star formation is triggered if the gas overdensity in a cell is greater than 50, ensuring that the first stellar particle appears at $z \sim 18$: once enabled, the star formation proceeds according to a Schmidt-Kenicutt Law with an efficiency of 1% (see Deparis et al. (2017) in prep.). The mass of a stellar particle is $7 \times 10^4 M_\odot$. It produces ionizing photons according to a Starburst 99 population model (Leitherer et al. 1999) with a Top-Heavy IMF and 0.05 $Z_\odot$ metallicity : the corresponding emissivity is 1.5×10^{17} ionising photons/sec/stellar kg for 3×10^6 years followed by an exponential decrease.

Furthermore, an in-situ 20% escape fraction is applied to compute the actual number of photons released in a simulation cell: it ensures a complete reionization at $z \sim 6$. Likewise, mechanical feedback is enabled and a typical energy of 9.8×10^{11} J/stellar kg is released in the surrounding gas after 15×10^6 years: 1/3 via thermal energy, 2/3 via kinetic winds. At z=6, 120×10^6 stellar particles are present.

The simulation required 32768 CPUs and 4096 graphics devices (GPUs) on the TITAN (ORNL/DOE) supercomputer. The EMMA code is partially ported on GPU, accelerating the hydrodynamics and the radiative transfer: these modules are respectively 25 and 15 times faster on GPU than a single CPU core. Provided that each GPU is shared by 8 cores and that a substantial part of EMMA is exclusively managed by CPUs, the addition of 4096 GPUs to the 32768 cores leads to an 1.5 acceleration factor. Finally, this simulation results from the conversion of a qualification run into a production one : it used a reduced speed of light ($c_{\rm sim} = 0.1c$) that has been kept for the final run.

The EMMA simulation stopped at $z = 6$: it presents a reionization epoch consistent with CMB constraints (Planck Collaboration et al. 2015) but with a residual neutral fraction at lower levels than expected from quasars data (Fan et al. (2006), see Fig. 1). The average star formation history is consistent with formation models obtained from the evolution of the high-z UV luminosity function (Bouwens et al. 2014; Finkelstein et al. 2015).

The properties of z=0 halos are obtained from a pure dark-matter Gadget simulation (Springel 2005), using the same initial conditions. Halos were identified using a FOF algorithm with a 0.2 linking length and minimal number of particles of 20, leading to ~ 20 millions structures identified at z=0. The smallest objects weigh $4 \times 10^7 M_\odot$. Merger trees were also produced to connect z=0 halos to their progenitors during the EoR. These $z \gg 0$ progenitors do not necessarily exist and only the largest z=0 halos have a progenitor identified 13×10^9 years earlier : 10^6 z=0 objects have an identified progenitor at z=6. Alternatively, all z=0 halos can be traced back to the Reionization using their particles which are uniquely identified.

2.3. *Reionization maps*

Reionization maps are built from the ionisation state of hydrogen : this quantity is computed self-consistently by the simulation code EMMA and we define the reionization time as the instant when a cell crosses the 0.5 ionized fraction threshold for the first time. The end result is a 3D field, $t_{\rm reion}(x, y, z)$, sampled using 2048^3 pixels corresponding to the base resolution of our simulations (see Fig. 2). When compared to the Gadget halo distribution at z=6, a clear correlation can be seen with the EMMA reionization map.

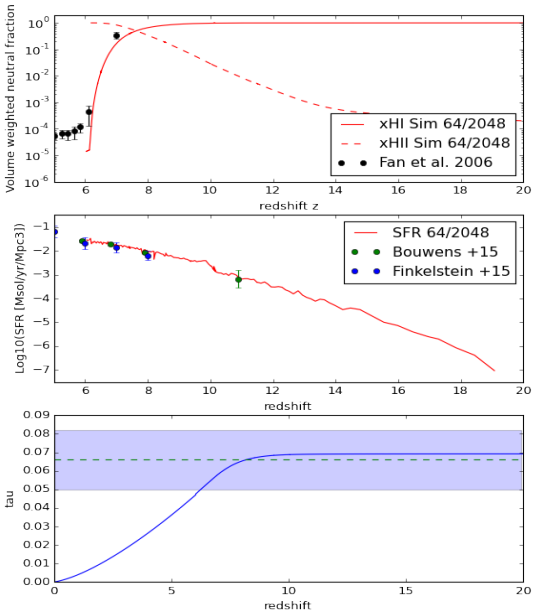

Figure 1. The global average properties of the simulations. From top to bottom : the volume averaged ionization/neutral fraction history, the cosmic star formation rate and the CMB thomson scattering optical depth.

This quantity is computed on the fly by EMMA with a time resolution driven by hydrodynamical processes. However due to memory management issues, this procedure had to be stopped at z=8 and reionization redshifts were computed from snapshots for the latest stages of the Reionization. At worse the time resolution is 1.4 Myrs at z=6.

2.4. *Progenitor based predictions*

This set of predictions is obtained from merger-trees of the DM-only simulation: they give access to z=6 progenitors of z=0 halos. In this approach, the reionization time of a $z = 0$ halo is given by

$$t_{\rm prog} = t_{\rm reion}(\vec{x}_{\rm mm6}), \quad (1)$$

where $\vec{x}_{\rm mm6}$ is the center-of-mass position of the most massive progenitor of this halo at z=6 (see Fig. 3).

A halo can be assigned a Reionization redshift only if it has a progenitor at z=6: this is not the case for halos that have emerged after z=6 or could not be detected by the FOF. However this procedure guarantees that $t_{\rm prog}$

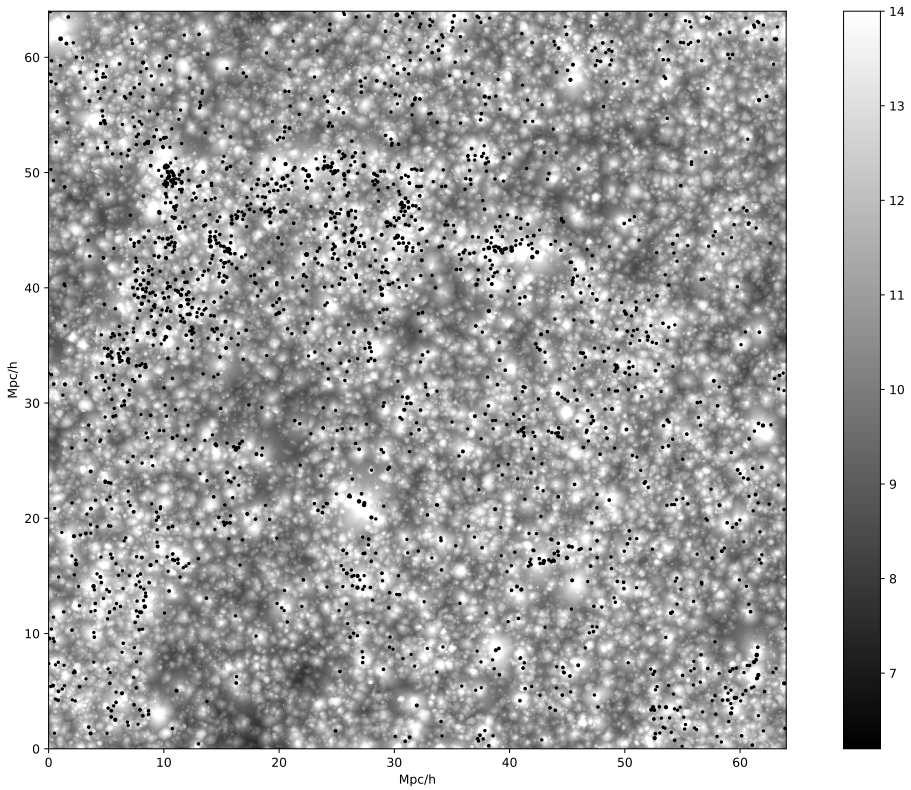

Figure 2. The projected spatial distribution of the 2000 most massive halos from the DM Gadget simulation at z=6 (symbols) and the maximum reionization redshift along the line of sight computed using EMMA.

is set by material already in place in the structure by z=6.

2.5. *Particle-based prediction*

This set of predictions is based on the halo-membership of each DM particle at z=0 (see Fig. 3). Once the list of particles that belong to a z=0 halo is established, their positions at z=6 can be traced-back from snaphots and each particle is then being assigned a reionization redshift. An average particle-based $t_{\rm part}$ can be assigned to each halo:

$$t_{\rm part} = \frac{\sum_{\vec{x}_{\rm p0}\in{\rm halo}} t_{\rm reion}(\vec{x}_{\rm p6})}{\sum_{\vec{x}_{\rm p0}\in{\rm halo}} 1}, \qquad (2)$$

where $\vec{x}_{\rm p0}$ and $\vec{x}_{\rm p6}$ are the $z = 0$ and $z = 6$ particles positions.

This procedure is more difficult to set up as it requires to cross-match 8×10^9 DM particles with $\sim 20\times10^6$ z=0 halos to assign particles to their halos.

However this technique is able to assign a reionisation redshift to all z=0 haloes, even the smallest ones. On the other hand, the halo reionisation times drift to later times since diffuse material, presumably reionized at later times and/or accreted after the Reionization, is taken into account.

3. RESULTS

3.1. *Reionization times*

The Reionization times of z=0 halos are shown in Fig. 4. Regardless of the methodology used, galaxies with $M_{z=0} > 10^{12}M_\odot$ reionize $\sim 150-250$ Myrs earlier than the full volume. In this mass range, the more massive the galaxies, the earlier they are reionized as expected since they host intense sources or are close to them in dense environments. At the lower masses ($M_{z=0} < 10^{12}M_\odot$) the Reionization time becomes consistent with the global one. The median time is slightly later than the global one : objects among this population are faint or even star-less and must be externally reionized. Being dense, it takes more time to reionize them than for the IGM. Nevertheless, the scatter is quite

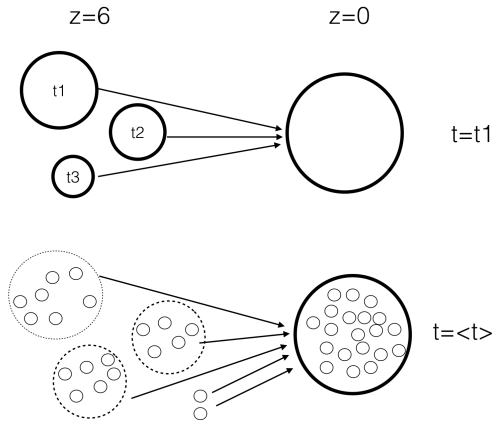

Figure 3. Assignments of the reionization times of z=0 halos. Top : the progenitor-based method considers $t_{\rm reion}$ of the most massive z=6 progenitor. Bottow : the particle-based method considers the average $t_{\rm reion}$ of all particles that end up in a z=0 halo.

significant from halo to halo ($\sim$ 240 Myrs 5%-95% percentile).

The two methodologies return consistent results but with differences. The progenitor-based technique guarantees that an object is already present at high z : it returns the reionization redshift of the oldest material of a z=0 halo, thus explaining why it consistently returns lower $t_{\rm reion}$. On the other hand it requires that objects detectable by means of FOF pre-exist at z=6, biasing the sample of halos: a $10^8 M_\odot$ halo at z=0 must have peculiar accretion rates to have a z=6 progenitor and still be small at z=0. The dip in reionization times at the low mass end confirms this and by eye inspection, these objects are located in high-density regions, thus explaining their low $t_{\rm reion}$. It could also indicate that these objects were more massive in the past and were disrupted : these low-mass objects are being assigned $t_{\rm reion}$ typical of more massive objects.

The particle-based methodology suffers less from this bias because all z=0 halos are considered : the $t_{\rm reion}$ dip at the low mass end disappears. However, it returns lower reionization redshifts for $M_{z=0} < 10^{11} M_\odot$, resulting from a fraction of material in halos at z=0 that was part of the diffuse matter in the IGM and was reionized at later times.

Li et al. (2014) found that $10^{12} M_\odot$ galaxies tend to reionize earlier than the IGM with $\Delta z \sim 1 \pm 1$ whereas we find earlier Reionization times for the same class of objects with $\Delta z \sim 2.5 \pm 2$. The differences could be related to methodologies : for instance they extrapolate reionization times using z=0 halos positions whereas we use z=6 progenitors or particle positions. While their approximation is appropriate for large halo mass

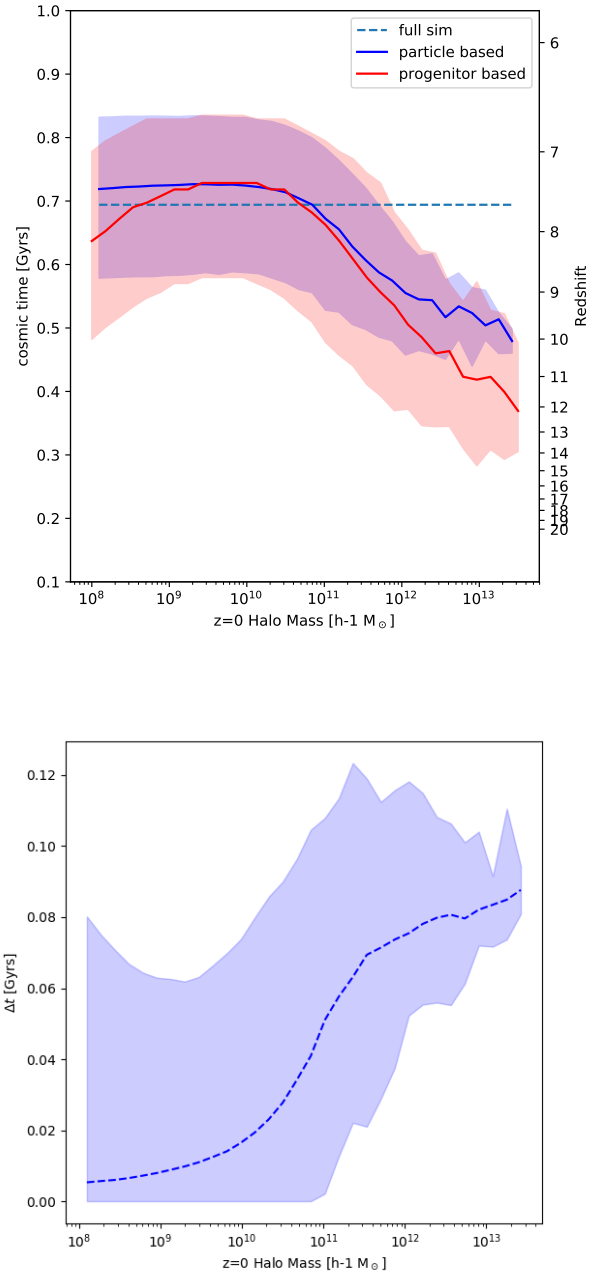

Figure 4. *Top*: The reionization time as a function of z=0 halo mass. Red stands for progenitor-based predictions while blue stands for particle-based predictions. The full volume reaches $x_{HI} = 0.5$ at $z \sim 7.8$ (dashed line). *Bottom*: The intrinsic duration of reionization Δt as a function of the halo mass. In both panels, lines stand for the median value within each bin of mass and shaded area cover the $5\% - 95\%$ percentiles.

($> 10^{12} M_\odot$), we found that z=0 positions are a poor approximation of the actual halo position at high z when

less massive objects are considered. Their reionization times closer to the global one could be a sign of 'signal dilution' at the lower-end of their probed range of halo mass. On the other hand, our initial conditions were designed to include large clusters in a relatively small volume : it could lead to an overestimate of the UV-background and an onset of the Reionization at earlier times than in their more representative large volumes.

3.2. *Durations of reionizations*

Using the particle-based method, we can investigate the intrinsic reionization duration Δt of $t_{\rm reion}$ within halos : its dependance on halo mass is shown in Fig. 4. Δt is computed by measuring the time interval between the 5 and 95 % percentile of the distribution of reionization times of all the particles that belong to a halo at z=0.

Δt increases with the halo mass with typical values of ~ 80 Myrs for $M_{z=0} > 10^{11} M_{\odot}$. Reionization durations as long as 120 Myrs or as short as 20 Myrs can be found. Ocvirk et al. (2014) made similar measurements on sub-haloes of M31-MW analogs and the current results are consistent with their SPH model that share a similar emissivity for the sources: the 80 Myrs duration found here is typical of their Reionization in isolation models, where an inside-out Reionization proceeds from the inner regions of a galaxy to its outskirts. Meanwhile the shortest $\Delta t = 20$ Myrs values are typical of their external reionization scenario, where a nearby bright source 'flashes' the object. The scatter seen here would be a reflection of diverse environmental properties.

For $M > 10^{11} M_{\odot}$, the typical values found for Δt are comparable to the halo-to-halo scatter of $t_{\rm reion}$: it's consistent with findings of Alvarez et al. (2009) and Li et al. (2014) for more massive objects. Consequently taking into account the variety of Reionization times to model the star formation in halos should also include the fact that within a halo the Reionization is not necessarily instantaneous.

At low mass end, $M_{z=0} < 10^{11} M_{\odot}$, objects have $\Delta t \sim 0$. It could correspond to extreme case of fast external reionizations or objects small enough to fit within a single cell of the Reionization map (the $30h^{-1}$ comoving kpc resolution corresponds to the virial radius of a $\sim 10^9 M_{\odot}$). The dispersion increases toward the low mass end : again it could be due to 'disrupted objects' which are being assigned Δt typical of more massive halos.

3.3. *Cosmic Variance*

As a crude environment dependence study, we split the simulation volume in 8 identical octants. We computed the z=6 average baryon density in each of these octants

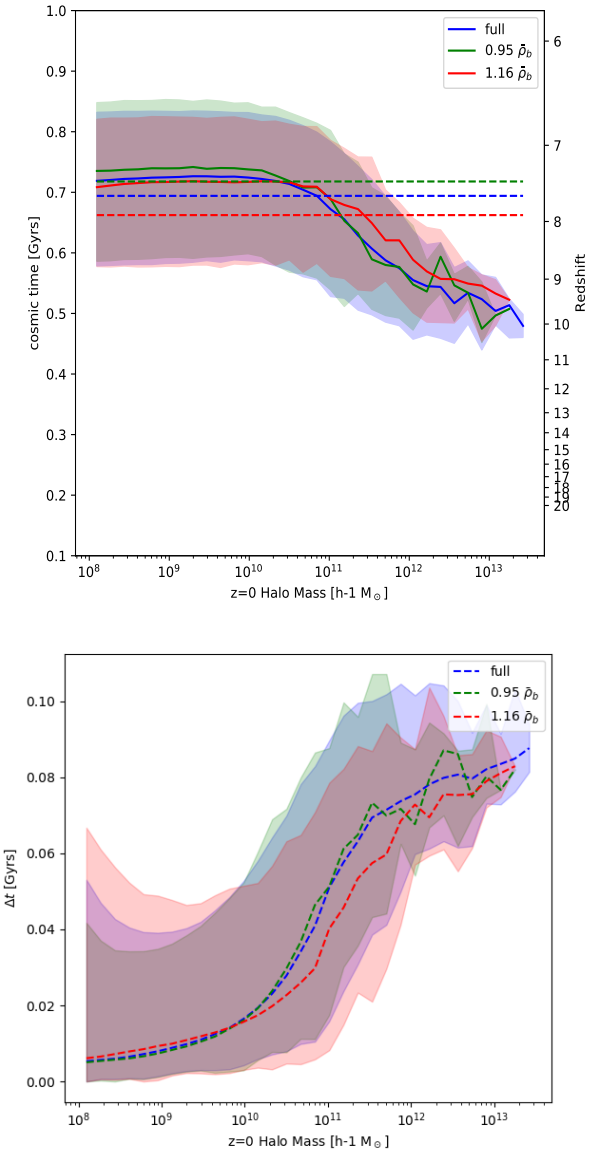

Figure 5. Reionization times (top) and durations (bottom) as function of halo mass in two different $32h^{-1}$ Mpc sub-volumes. Green/red stand for the most underdense/overdense octant. Blue stands for quantities computed in the full $64h^{-1}$ Mpc volume. Lines stand for the median values in each bin of mass while the shaded area cover the $5\% - 95\%$ percentiles. Dashed lines in the top panel stand for the reionization times of each sample.

and considered the most overdense (with $\rho_b \sim 1.19\bar{\rho}_b$) and underdense ones (with $\rho_b \sim 0.95\bar{\rho}_b$). In these octants, we recomputed the particle-based reionization times and durations (see Fig. 5).

The scatter remains quite important, these two octants present compatibles trends and are both consis-

tent with the one obtained from the full box. There are subtle differences nevertheless. At the low mass end, the denser the volume the lower are the reionization times as expected : a dense volume should host bright and rare sources thus promoting an early reionization. At the high mass end however, the opposite trend can be seen : the densest octant promotes surprisingly lower reionization redshifts. It could be a small number effect which prevent convergence of these results or due to the moderation of star formation by the brightest sources in these densest environments : the largest and brightest sources would lower the photon production of less massive objects that provide the majority of ionizing photons. The net result would be a later onset of Reionization in these regions.

In Fig. 5, we also present the same sub-volume dependence for reionization durations Δt. Halos in the densest octant are reionized in a more sudden manner compared to the low density sub-box and to the full volume. It's consistent with the promotion of fast external Reionizations relative to internal ones in more clustered environments. As expected, both results on $t_{\rm reion}$ and Δt suggest that environment effects have a role to play.

4. DISCUSSION

Our simulations predict that halos between 10^8 and $10^{13} M_\odot$ have a biased perception of the Reionization : for MW-like objects, it occurs 150 Myrs before the full volume with a $\sim$ 100 Myrs scatter. The scatter within a halo can be as large as the halo-to-halo variation, implying that any modeling that include the latter should include fluctuations of Reionization times within a galaxy for consistency.

Our results complement investigations made by e.g. Alvarez et al. (2009), Li et al. (2014) and Ocvirk et al. (2014). In Ocvirk et al. (2014), sub-haloes of M31 and MW analogs display a radial gradient of reionization redshift in their z=0 distribution : noting that our data display a similar spatial resolution, the statistics of such gradients in a population of MW-Like objects can be studied. They would depend on the environment of halos, as implied by the wide variety of Reionization durations and by the comparisons between sub-volumes : further investigations are under way.

Our choices can impact our predictions. The resolution achieved here could only be obtained on moderate cosmological volumes, compared to e.g. Li et al. (2014). Such volumes are known to limit the representativity of HII regions sizes (see e.g. Iliev et al. (2006)) and underestimate the spatial fluctuation levels of Reionization fields. Also, our initial conditions were designed to produce analogs of Local clusters : our Reionization is therefore unlikely to be fully representative of the transition experienced by a randomly selected 64 Mpc volume .

Finally, the current work is the result of a long-term development strategy and challenging productions runs, but the physics included here remain quite limited. The inclusion of AGNs would lead to another sources of environmental fluctuations (see e.g. Chardin et al. (2015)), whereas more complete models for star formation (driven by molecular or metal cooling, see e.g. Wise & Cen (2009)) are expected to modify the repartition of photons production among the halo classes. All these effects are expected to modify our quantitative predictions for halos Reionization times and duration. On the other hand, this work in conjunction to previous ones establish further the biased and diverse view of the Reionization as seen by galaxies : a more complete modeling is unlikely to modify this conclusion.

ANR ORAGE, ANR EMMA, INCITE Project, ORNL Staff, etc...

REFERENCES

Alvarez, M. A., Busha, M., Abel, T., & Wechsler, R. H. 2009, ApJL, 703, L167

Aubert, D., Deparis, N., & Ocvirk, P. 2015, MNRAS, 454, 1012

Bouwens, R. J., Bradley, L., Zitrin, A., et al. 2014, ApJ, 795, 126

Brown, T. M., Tumlinson, J., Geha, M., et al. 2014, ApJ, 796, 91

Busha, M. T., Alvarez, M. A., Wechsler, R. H., Abel, T., & Strigari, L. E. 2010, ApJ, 710, 408

Chardin, J., Haehnelt, M. G., Aubert, D., & Puchwein, E. 2015, MNRAS, 453, 2943

Deparis, N., Aubert, D., Ocvirk, P., & Gillet, N. 2017, in prep., arXiv:1005.2687

Fan, X., Carilli, C. L., & Keating, B. 2006, ARA&A, 44, 415.

Finkelstein, S. L., Ryan, Jr., R. E., Papovich, C., et al. 2015, ApJ, 810, 71

Gillet, N., Ocvirk, P., Aubert, D., et al. 2015, ApJ, 800, 34

Gottloeber, S., Hoffman, Y., & Yepes, G. 2010, ArXiv e-prints, arXiv:1005.2687

Hinshaw, G., Weiland, J. L., Hill, R. S., et al. 2009, ApJS, 180,225

Iliev, I. T., Mellema, G., Pen, U.-L., et al. 2006, MNRAS, 369, 1625

Iliev, I. T., Moore, B., Gottlöber, S., et al. 2011, MNRAS, 413, 2093

Koposov, S. E., Yoo, J., Rix, H.-W., et al. 2009, ApJ, 696, 2179

Leitherer, C., Schaerer, D., Goldader, J. D., et al. 1999, ApJS, 123, 3.

Li, T. Y., Alvarez, M. A., Wechsler, R. H., & Abel, T. 2014, ApJ, 785, 134

Ocvirk, P., & Aubert, D. 2011, MNRAS, 417, L93

Ocvirk, P., Gillet, N., Aubert, D., et al. 2014, ApJ, 794, 20

Ocvirk, P., Gillet, N., Shapiro, P. R., et al. 2016, MNRAS, 463, 1462

Planck Collaboration, Ade, P. A. R., Aghanim, N., et al. 2015, ArXiv e-prints, 1502, arXiv:1502.01589.

Springel, V. 2005, MNRAS, 364, 1105

Wise, J. H., & Cen, R. 2009, ApJ, 693, 984